Supplementary Information – "Mineralogical characteristics influence the structure and pozzolanic reactivity of thermally and mechano-chemically activated meta-kaolinites"

Alastair T.M. Marsh[a*]; Andy P. Brown[b]; Helen M. Freeman[a]; Anke Neumann[c,d]; Brant Walkley[e]; Helen Pendlowski[f]; Susan A. Bernal[a]

[a] School of Civil Engineering, University of Leeds, Leeds LS2 9JT, United Kingdom
[b] School of Chemical and Process Engineering, University of Leeds, Leeds LS2 9JT, United Kingdom
[c] Paul Scherrer Institut, 5232 Villigen PSI, Switzerland
[d] School of Engineering, University of Newcastle upon Tyne, NE1 7RU, United Kingdom
[e] Department of Chemical and Biological Engineering, University of Sheffield, Sheffield, United Kingdom
[f] The James Hutton Institute, Craigiebuckler, Aberdeen, United Kingdom
* corresponding author: a.marsh@leeds.ac.uk

S1. Activation energy of kaolinite dehydroxylation

The activation energy of dehydroxylation for the kaolinite in the LoFe clay and the HiFe clay was calculated by conducting thermogravimetric measurements over a range of heating rates of 1-20°C/min (Figure S1), and then using the temperature of the dehydroxylation peak to construct Kissinger plots (Figure S2). From the Kissinger plots, the activation energy of dehydroxylation (Table S1) was calculated as described in the Methods section of the main article.

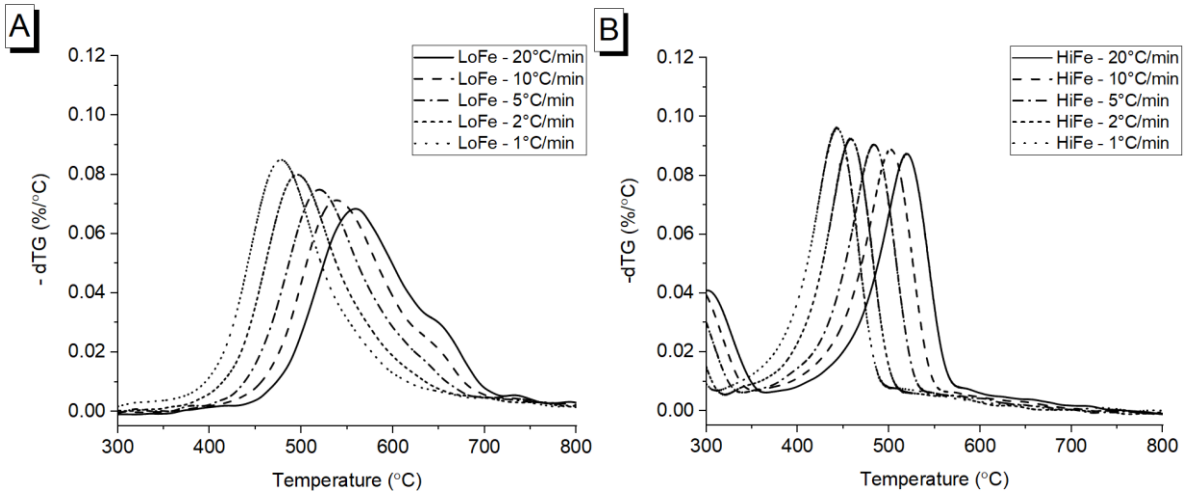

Figure S1: Differential thermogravimetric curves at heating rates of 1-20°C/min, for the as-received A) LoFe and B) HiFe clays.

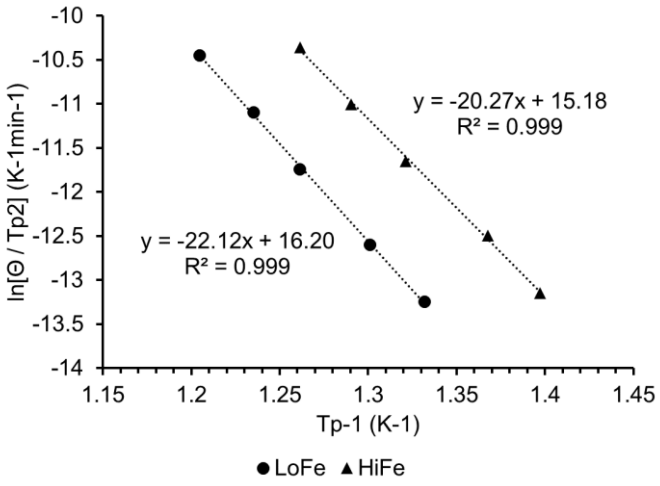

Figure S2: Kissinger plots for the as-received LoFe and HiFe clays.

Table S1: Summary of key thermal parameters for the as-received LoFe and HiFe clays.

Clay	Activation energy of dehydroxylation ($kJmol^{-1}$)	Dehydroxylation peak temperature (at 10°C/min heating rate) (°C)
LoFe	183.9	538.6
HiFe	168.5	501.9

S2. Further discussion of changes to kaolinite and associated minerals after activation

For kaolinites, there is conventionally a direct, inextricable link made between dehydroxylation and amorphisation. However, considering the behaviours observed in Section 3.1 of the main article for kaolinites with different mineralogical characteristics, under different processing routes, there are nuances to the relationship between dehydroxylation and amorphization of kaolinites. For HiFe-therm, the XRD pattern (Figure 1B) and FTIR spectrum (Figure 3C) (and potentially also the EEL spectrum (Figure 8B)) indicated some retention of kaolinite structure and structural hydroxyls after thermal activation, despite its TG curve indicating complete dehydroxylation (Figure 2D). For LoFe-mech, the XRD pattern (Figure 1A) indicated complete amorphization of the kaolinite structure, but the FTIR spectrum (Figure 3A) indicated minor retention of structural hydroxyls. These subtle behaviours may not necessarily have practical importance for application in low-carbon cement production, but are a reminder that kaolinite dehydroxylation is yet to be fully understood on a fundamental level [1].

The XRD patterns of the as-received clays, the thermally-activated clays and the mechano-chemically activated clays are shown in Figure 1 in the main article. The discussion in the main article focusses on the changes to the diffraction peaks of kaolinite in both clays, and also muscovite in the LoFe clay and goethite in the HiFe clay, as these associated minerals have the highest mass fraction in each as-received clay. The following paragraphs describe the effects of both activation treatments on the other associated minerals in both clays.

For the LoFe clay, detectable gibbsite reflections were no longer observed in the LoFe-therm XRD pattern – it is expected that gibbsite underwent thermal decomposition during the calcination process[2] ($Al(OH)_3 \rightarrow Al_2O_3 + H_2O$) . However, no detectable corundum reflections were observed in the LoFe-therm XRD pattern. K-feldspar diffraction peaks were still observed in both the LoFe-therm and LoFe-mech XRD patterns, indicating that its structure was not greatly affected by either activation treatment. Quartz did not experience any obvious changes in its diffraction peaks' profile after either treatment. Some amorphization of quartz is possible, but requires a longer milling duration than that used in this study [3].

For the HiFe clay, anatase diffraction peaks were still present in the HiFe-therm XRD pattern, but no detectable peaks were observed in the HiFe-mech pattern, suggesting destruction of long-range order. Alongside goethite, minor quantities of hematite and magnetite or maghemite were also present in the HiFe clay. Given that goethite was dehydrated to hematite after activation (to completion for HiFe-therm, and to a partial extent for HiFe-mech), it is not possible to distinguish the starting hematite from the hematite that resulted from activation. A very small quantity of magnetite or maghemite was present in the HiFe clay, with a weak, non-overlapping peak detectable at 30.2 °2θ. At a calcination temperature of 750°C, it is expected that magnetite (if present) will undergo oxidation to form hematite[2] ($4Fe_3O_4 + O_2 \rightarrow 6Fe_2O_3$). No detectable magnetite peak was present in the HiFe-therm pattern, indicating that oxidation did take place during the thermal treatment. It is not known whether intensive milling using the conditions in this study is likely to cause oxidation of magnetite (if present). It is not possible to say with confidence whether the weak, non-overlapping peak at 30.2 °2θ was detectable in the HiFe-mech pattern or not.

S3. Changes to aluminosilicate framework adsorption bands after activation

The FTIR spectra of the as-received clays, the thermally-activated clays and the mechano-chemically activated clays are shown in Figure 3 in the main article. The discussion in the main article focusses on the changes to the adsorption bands corresponding to structural hydroxyls and surface-adsorbed water in the 3000 – 3800 cm^{-1} wavenumber range. The following paragraph describes the effects of both activation treatments on adsorption bands associated with the aluminosilicate framework, in the 600 – 1200 cm^{-1} wavenumber range.

Al-O-H and Si-O bands, corresponding to vibrations within the octahedral and tetrahedral sheets of kaolinite respectively, were clearly resolved in the 650-1200 cm^{-1} range for the LoFe and HiFe clay's spectra (Figure 3B,D in the main article). The presence of a small amount of quartz within both the LoFe and HiFe clays is expected to make a minor contribution to the Si-O bands at 775 and 798 cm^{-1}. Significant broadening, and also an extent of intensity reduction, was observed for the Al-O-H bending and Si-O stretching bands after both treatments, indicative of increased structural disorder within the aluminosilicate framework of kaolinite [4]. This is consistent with the changes observed in the XRD patterns (Figure 1 in the main article).

S4. Particle size reduction of clays after mechano-chemical treatment

The particle size reduction at the <1 μm scale was far more extensive for HiFe-mech compared to LoFe-mech - this can be explained by the different ranges of particle size and hardness of

the constituent minerals. Of the minerals in the LoFe as-received clay, muscovite has similar hardness as kaolinite (Mohs hardness = 2.5), and quartz is by far the hardest mineral (Mohs hardness = 7). Quartz is a primary mineral commonly occurring in clays and soils that is resistant to weathering; as a result it typically has a coarser particle size distribution than clay minerals (usually in the silt size fraction, defined as 2-50 μm) [5], including in hydrothermal kaolins such as the LoFe clay [6]. The LoFe clay thus represents the most commonly encountered configuration of minerals previously investigated in intensive milling: of the major minerals, kaolinite is the finest and also the softest, whilst quartz is the hardest, with a comparable or larger particle size. Mako et al. [7] showed that an increased content of quartz accelerated the dehydroxylation and amorphization of kaolinite; however, the relative increase in specific surface area was lower with increased additions of quartz. In that study, the quartz addition had a very similar size distribution to the kaolinitic clay itself (majority of particles between 1-10 μm). Of the minerals in the as-received HiFe clay, the TEM images and STEM-EDX maps show that the goethite particles (<10 nm) are noticeably smaller than the kaolinite particles (>100 nm). Goethite (Mohs hardness = 5 - 5.5) and hematite (Mohs hardness = 5 - 6), into which goethite was partially transformed during the mechano-chemical treatment, are harder minerals than kaolinite (Mohs hardness = 2 - 2.5). The HiFe-clay represents the opposite situation to the LoFe clay – of the major minerals, kaolinite is the softest, but also the largest; whereas goethite (and hematite), are the hardest but also the smallest. The particle size data indicates that goethite and hematite particles enhanced comminution of kaolinite in the HiFe clay to a greater extent than quartz in the LoFe clay, presumably due to the extremely fine size of the goethite and hematite. It is challenging to draw out generalised trends in comminution given the dependence of particle breakage phenomena on the relative volumes of coarse and fine fractions [8], the density and hardness of minerals, and mill operating conditions [9]. The explanation presented here is plausible, but would need further research to confirm.

S5. N_2 sorption and porosity characteristics of as-received and activated clays

All the clays' N_2 sorption isotherms were Type IVa type, which is typical for clays with plate-like particles [10] (Figure S3). All isotherms exhibited an adsorption-desorption hysteresis loop, which most closely matches the H3 hysteresis loop type [10]. The isotherms for LoFe-therm (Figure S3B) and LoFe-mech (Figure S3C) had a very similar profile to as-received LoFe (Figure S3A). As-received HiFe had a much higher adsorptive capacity (108.1 cm^3/g STP) than as-received LoFe (26.6 cm^3/g STP); HiFe also had a much wider hysteresis loop than LoFe. The isotherm profile of HiFe-therm (Figure S3E) was very similar to HiFe (Figure S3D); however, HiFe-mech had a much lower adsorptive capacity (24.6 cm^3/g STP) and narrower hysteresis loop, with an isotherm profile more similar to the LoFe series clays than the other HiFe series clays.

Making accurate, quantitative measurements of mesoporosity (defined as pores with width between 2 – 50 nm [10]) using N_2 sorption offers several challenges, especially for samples with low total volumes of porosity [11]. Nonetheless, N_2 sorption isotherms can be used to give a qualitative indication of whether the clays underwent any major changes in mesoporosity after the activation treatments – in particular, for the mechano-chemically activated clays, which underwent a significant change in morphology (Figure 5 in main article). LoFe-mech showed a modest reduction in cumulative pore volume compared to both LoFe and LoFe-therm (Figure S4A). HiFe-mech showed a substantial reduction in cumulative pore volume compared to HiFe (Figure S4B), potentially indicative of denser aggregates.

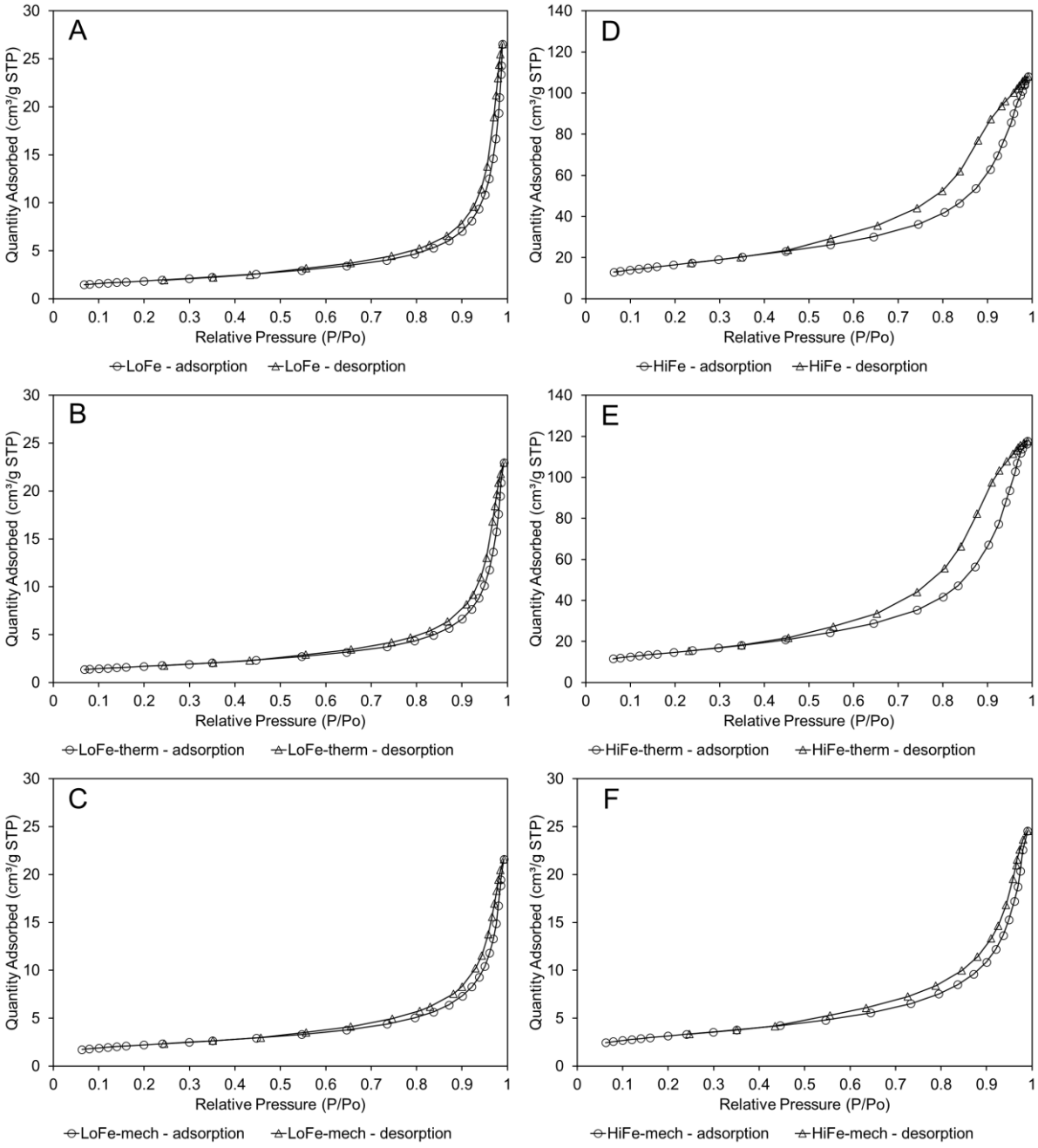

Figure S3: N_2 sorption isotherms for A) LoFe; B) LoFe-therm; C) LoFe-mech; D) HiFe; E) HiFe-therm; F) HiFe-mech. Note the lower y-axis limit for F) compared to D) and E). STP = at standard temperature and pressure.

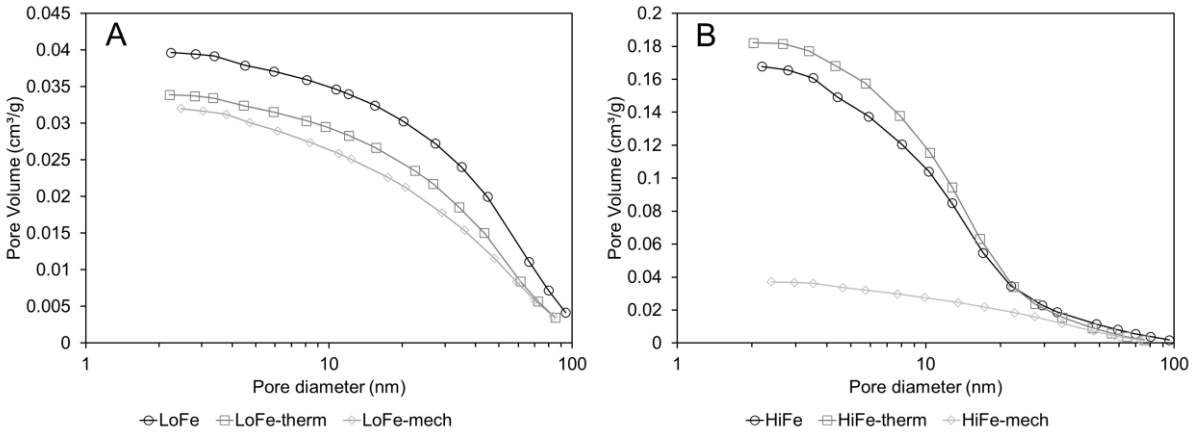

Figure S4: Cumulative pore volume curves, calculated using the Barrett, Joyner and Halenda (BJH) method [12] from the desorption isotherm, for A) LoFe clay series, and B) HiFe clay series.

S6. R^3 reactivity classification and implications for use in blended cements

Using the RILEM TC-TRM scheme to classify the 7-day cumulative values [13], LoFe-therm (798.5), LoFe-mech (702.1), HiFe-therm (584.2) and HiFe-mech (513.6) were all clearly within the boundaries of a "moderately reactive" calcined clay (i.e. 90% probability threshold > 190 J / g of activated clay), but falling short of the requirements for a "highly reactive" calcined clay (i.e. a 66% probability threshold > 800 J / g of activated clay). For the as-received clays, HiFe (83.0 J / g of clay) evolved greater 7-day cumulative heat than LoFe (4.4 J / g of clay) (Figure S5).

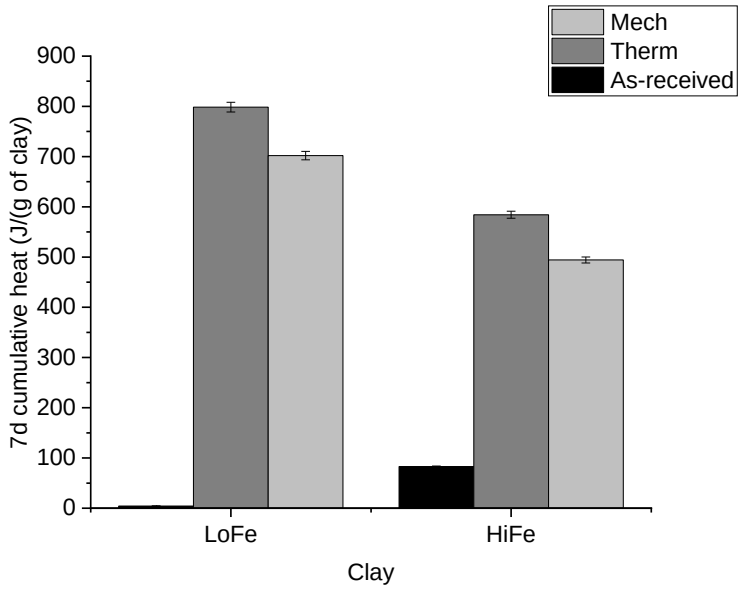

Figure S5: 7-day cumulative heat values obtained from the R3 test. Error bars represent 1.2% of the 7-day cumulative heat; the single operator coefficient of variance was determined to be 1.2% from interlaboratory tests on a calcined clay [14].

The lower 7 day reactivity of mechano-chemically activated kaolinitic clays indicates that the viable substitution levels of mechano-chemically activated clay for clinker replacement in a

blended cement would be lower than for a thermally activated kaolinitic clay (to achieve equivalent strength development at 7 days and beyond). However, the strength development of blended cements depends on multiple factors beyond solely chemical reactivity of the supplementary cementitious material. The influence of mechano-chemically activated kaolinitic clays' retained water and fine particle size distribution on blended cements' workability and particle packing, and hence strength development, remains an open question.

S7. Anhydrous meta-kaolinite content of activated clays

The content of anhydrous meta-kaolinite in the activated clays was calculated, in order to compare cumulative heat per gram of anhydrous meta-kaolinite (Figure 11 in main article). The overall approach was to calculate the mass of anhydrous meta-kaolinite in 100 g of each as-received clay, and the mass of each activated clay from a starting mass of 100 g of as-received clay, and then divide the two values to obtain the mass fraction of anhydrous meta-kaolinite in each activated clay. A schematic diagram of this approach is given below (Figure S6), followed by descriptions of the calculation procedure for both activation routes.

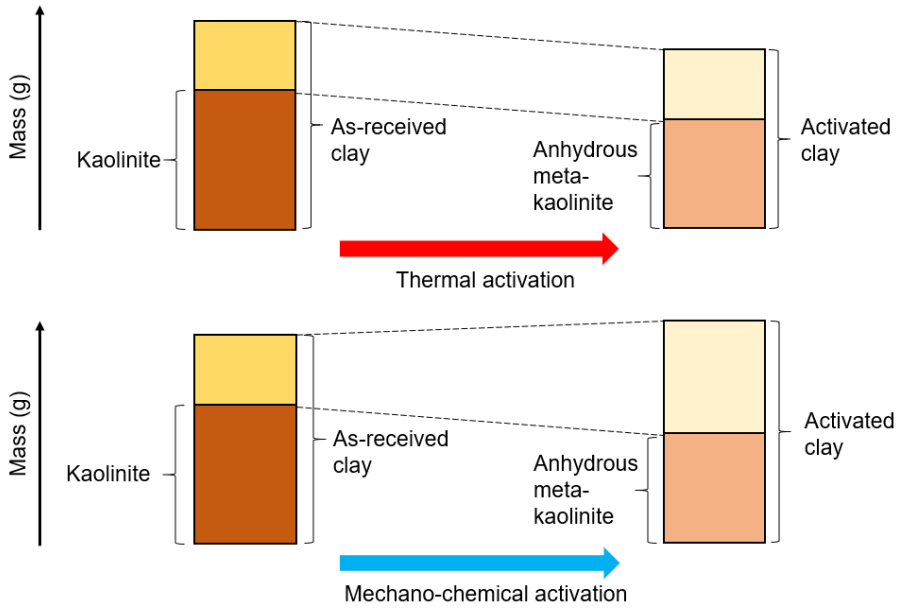

Figure S6: Schematic diagram showing the changes in mass from the as-received clay to the activated clay, and from kaolinite content to anhydrous meta-kaolinite, for thermal activation and mechano-chemical activation.

The kaolinite content of both the LoFe clay and HiFe clays was determined by quantitative XRD analysis, which then gives the mass of kaolinite per 100 g of as-received clay. From this point, calculating the yield of activated clay from 100 g of as-received clay is different for the thermal and mechano-chemical activation routes.

For thermal activation, the mass yield of thermally-activated clay was estimated from the mass% value of the thermogravimetric curve of the as-received clay at 750°C (Figure 2A,D in main article), the temperature of calcination. The mass of anhydrous meta-kaolinite was then estimated by multiplying the mass of kaolinite in 100 g of as-received clay, by the theoretical anhydrous mass proportion of kaolinite (i.e. after removal of structural hydroxyls) of 86 wt.% [15]. Then, the mass of anhydrous meta-kaolinite was divided by the mass yield of

thermally activated clay, to give the proportion of anhydrous meta-kaolinite in thermally activated clay. Values are given below in Table S2.

Table S2: Values used to calculate the proportion of anhydrous meta-kaolinite in thermally activated LoFe and HiFe clays.

Parameter	**LoFe clay**	**HiFe clay**
Kaolinite content in as-received clay	73.5 wt.%	62.7 wt.%
Mass of kaolinite in 100g of as-received clay	73.5 g	62.7 g
Yield of thermally activated clay from 100 g of as-received clay	89.4 g	86.3 g
Mass of anhydrous kaolinite after thermally activating 100 g of as-received clay	63.2 g	53.9 g
Proportion of anhydrous meta-kaolinite in thermally activated clay	70.7 wt.%	62.5 wt.%

For mechano-chemical activation, a different approach to calculating yield mass was required, given that the intensive milling occurred in a closed system and so moisture released from dehydroxylation was retained. As seen in the thermogravimetric curves (Figure 2A,D in the main article), mechano-chemical activation resulted in slightly higher mass loss at 1000°C compared to the as-received clays. This was attributed to additional adsorption of atmospheric moisture during the milling process. The proportion of additional mass gain was estimated from the extra mass loss of each mechano-chemically activated clay, compared to the respective as-received clay, at 1000°C in the thermogravimetric curves. Adding this mass gain onto the 100 g of as-received clay gave the mass yield of activated clay. The mass of anhydrous meta-kaolinite was then estimated in the same way as described above for thermal activation. Then, the mass of anhydrous meta-kaolinite was divided by the mass yield of mechano-chemically activated clay, to give the proportion of anhydrous meta-kaolinite in mechano-chemically activated clay. Values are given below in Table S3.

Table S3: Values used to calculate the proportion of anhydrous meta-kaolinite in mechano-chemically activated LoFe and HiFe clays.

Parameter	**LoFe clay**	**HiFe clay**
Kaolinite content in as-received clay	73.5 wt.%	62.7 wt.%
Mass of kaolinite in 100g of as-received clay	73.5 g	62.7 g
Mass gain during mechano-chemical activation	1.3 wt.%	2.4 wt.%
Yield of mechano-chemically activated clay from 100 g of as-received clay	101.3 g	102.4 g
Mass of anhydrous kaolinite after mechano-chemically activating 100 g of as-received clay	63.2 g	53.9 g
Proportion of anhydrous meta-kaolinite in mechano-chemically activated clay	62.4 wt.%	52.7 wt.%

S8. Mössbauer hyperfine parameters

The hyperfine spectral parameters obtained from the Mössbauer spectra for the as-received and activated Fe-rich clays (Figure 12 in the main article) are stated in Table S4.

Table S4: Mössbauer hyperfine parameters of HiFe clay as-received (HiFe), after thermal treatment (HiFe-therm) and after mechanical treatment (HiFe-mech). Spectra were acquired at room temperature (293 K) and at 4 K and were evaluated for Mössbauer parameters using a Voigt-based fitting routine[16].

		RT: 293 K					LHT: 4 K				
sample	**component**	**<CS>**[b]	**<|QS|> or <ε>**[c]	**<|H|>**[d]	**σ(|H| or |QS|)**[e]	**Area (σ)**[f]	**<CS>**[b]	**<|QS|> or <ε>**[c]	**<|H|>**[d]	**σ(|H| or |QS|)**[e]	**Area (σ)**[f]
(χ^2)[a]		mm/s	mm/s	T	T or mm/s	%	mm/s	mm/s	T	T or mm/s	%
HiFe	Fe(III) doublet	0.36	0.65		0.33	71.9 (1.4)	0.45	0.61		0.29	5.0 (0.2)
(0.64/6.07)	Fe(III): goethite						0.48	-0.11	49.1	2.2	79.9 (0.1)
	Fe(III): hematite	0.36	-0.11	50.0	2.2	28.1 (1.4)	0.48	-0.08	53.1	0.7	15.1 (0.1)
HiFe-therm	Fe(III) doublet	0.37	1.07		0.61	12.3 (0.5)	0.51	1.73		0.84	5.9 (0.1)
(1.17/11.1)	Fe(III): hematite	0.37	-0.11	49.1	2.9	87.7 (0.5)	0.48	-0.10	52.4	1.5	94.1 (0.1)
HiFe-mech	Fe(III) doublet	0.36	0.77		0.41	63.0 (2.6)	0.46	1.09		0.50	8.2 (0.2)
(1.06/10.7)	Fe(III): collapsed	0.29	-0.03	15.2	6.8	19.3 (2.9)	0.77	-0.09	22.4	3.5	6.2 (0.3)
	Fe(III): goethite						0.48	-0.09	48.8	3.0	70.8 (0.9)
	Fe(III): hematite	0.37	-0.04	48.6	5.4	17.8 (1.3)	0.49	-0.08	52.9	0.7	14.8 (1.0)

[a]Reduced chi-squared value for the fit of the data collected at 293 K / collected at 4 K. [b]Centre shift relative to α-Fe(0). [c]Average quadrupole split value of a doublet (QS) or average quadrupole shift value of a sextet (ε). [d]Average magnetic field of the hyperfine field magnetic distribution (sextet). [e]Standard deviation width of the QS or H distribution. [f]Standard deviation due to uncertainty.

References

1. M. Izadifar, P. Thissen, A. Steudel, R. Kleeberg, S. Kaufhold, J. Kaltenbach, R. Schuhmann, F. Dehn and K. Emmerich, *Clays and Clay Minerals*, 2020, **68**, 319-333.
2. M. Földvári, *Handbook of the thermogravimetric system of minerals and its use in geological practice*, Geological Institute of Hungary, Budapest, Hungary, 2011.
3. K. Gobindlal, Z. Zujovic, P. Yadav, J. Sperry and C. C. Weber, *The Journal of Physical Chemistry C*, 2021, **125**, 20877-20886.
4. R. L. Frost, É. Makó, J. Kristóf, E. Horváth and J. T. Kloprogge, *Journal of Colloid and Interface Science*, 2001, **239**, 458-466.
5. M. Nanzyo and H. Kanno, in *Inorganic Constituents in Soil: Basics and Visuals*, eds. M. Nanzyo and H. Kanno, Springer Singapore, Singapore, 2018, pp. 11-35.
6. A. Psyrillos, C. Manning David A and D. Burley Stuart, *Journal of the Geological Society*, 1998, **155**, 829-840.
7. É. Makó, R. L. Frost, J. Kristóf and E. Horváth, *Journal of Colloid and Interface Science*, 2001, **244**, 359-364.
8. D. W. Fuerstenau and A. Z. M. Abouzeid, *International Journal of Mineral Processing*, 1991, **31**, 151-162.
9. V. K. Gupta, *Powder Technology*, 2020, **375**, 549-558.
10. M. Thommes, K. Kaneko, A. V. Neimark, J. P. Olivier, F. Rodriguez-Reinoso, J. Rouquerol and K. S. W. Sing, *Pure and Applied Chemistry*, 2015, **87**, 1051-1069.
11. M. F. De Lange, T. J. H. Vlugt, J. Gascon and F. Kapteijn, *Microporous and Mesoporous Materials*, 2014, **200**, 199-215.
12. E. P. Barrett, L. G. Joyner and P. P. Halenda, *Journal of the American Chemical Society*, 1951, **73**, 373-380.
13. D. Londono-Zuluaga, A. Gholizadeh-Vayghan, F. Winnefeld, F. Avet, M. Ben Haha, S. A. Bernal, Ö. Cizer, M. Cyr, S. Dolenec, P. Durdzinski, J. Haufe, D. Hooton, S. Kamali-Bernard, X. Li, A. T. M. Marsh, M. Marroccoli, M. Mrak, Y. Muy, C. Patapy, M. Pedersen, S. Sabio, S. Schulze, R. Snellings, A. Telesca, A. Vollpracht, G. Ye, S. Zhang and K. L. Scrivener, *Materials and Structures*, 2022, **55**, 142.
14. F. Avet, X. Li, M. Ben Haha, S. A. Bernal, S. Bishnoi, Ö. Cizer, M. Cyr, S. Dolenec, P. Durdzinski, J. Haufe, D. Hooton, M. C. G. Juenger, S. Kamali-Bernard, D. Londono-Zuluaga, A. T. M. Marsh, M. Marroccoli, M. Mrak, A. Parashar, C. Patapy, M. Pedersen, J. L. Provis, S. Sabio, S. Schulze, R. Snellings, A. Telesca, M. Thomas, F. Vargas, A. Vollpracht, B. Walkley, F. Winnefeld, G. Ye, S. Zhang and K. Scrivener, *Materials and Structures*, 2022, **55**, 92.
15. R. C. Mackenzie and S. Caillère, in *Soil Components: Vol. 2: Inorganic Components*, ed. J. E. Gieseking, Springer Berlin Heidelberg, Berlin, Heidelberg, 1975, pp. 529-571.
16. D. G. Rancourt and J. Y. Ping, *Nuclear Instruments and Methods in Physics Research Section B: Beam Interactions with Materials and Atoms*, 1991, **58**, 85-97.